



Swansea University
Prifysgol Abertawe



Cronfa - Swansea University Open Access Repository

This is an author produced version of a paper published in :

The Aeronautical Journal

Cronfa URL for this paper:

<http://cronfa.swan.ac.uk/Record/cronfa31571>

Paper:

Griffiths, L., Gaitonde, A., Jones, D. & Friswell, M. (2016). A pulse size estimation method for reduced-order models.

The Aeronautical Journal, 120(1234), 1891-1916.

<http://dx.doi.org/10.1017/aer.2016.111>

This article is brought to you by Swansea University. Any person downloading material is agreeing to abide by the terms of the repository licence. Authors are personally responsible for adhering to publisher restrictions or conditions. When uploading content they are required to comply with their publisher agreement and the SHERPA RoMEO database to judge whether or not it is copyright safe to add this version of the paper to this repository.

<http://www.swansea.ac.uk/iss/researchsupport/cronfa-support/>

A Pulse Size Estimation Method for Reduced Order Models

L.M. Griffiths

A.L. Gaitonde*

D.P. Jones

University of Bristol
Department of Aerospace Engineering,
Bristol
UK

M.I. Friswell

University of Swansea
College of Engineering
Swansea
UK

ABSTRACT

Model order reduction (MOR) is an important technique that allows reduced order models (ROMs) of physical systems to be generated that can capture the dominant dynamics, but at lower cost than the full order system. One approach to MOR that has been successfully implemented in fluid dynamics is the Eigensystem Realization algorithm (ERA). This method requires only minimal changes to the inputs and outputs of a CFD code so that the linear responses of the system to unit impulses on each input channel can be extracted. One of the challenges with the method is to specify the size of the input pulse. An inappropriate size may cause a failure of the code to converge due to non-physical behaviour arising during the solution process. This paper addresses this issue by using piston theory to estimate the appropriate input pulse size.

* Corresponding author: ann.gaitonde@bristol.ac.uk

NOMENCLATURE

a	local speed of sound
\mathbf{a}	the position vector of a point on the aerofoil surface
\mathbf{a}_x	is the position vector of the centre of pitch rotation
$\mathbf{A}, \mathbf{B}, \mathbf{C}, \mathbf{D}$	continuous linear state-space system matrices
$\tilde{\mathbf{A}}, \tilde{\mathbf{B}}, \tilde{\mathbf{C}}$	discrete linear state-space system matrices
$\tilde{\mathbf{A}}_r, \tilde{\mathbf{B}}_r, \tilde{\mathbf{C}}_r$	reduced discrete linear state-space system matrices
\mathbf{b}	the position vector of a point on the flap surface
\mathbf{b}_x	is the position vector of the flap hinge centre of rotation
c	aerofoil chord
C_d	drag coefficient
C_h	flap hinge moment coefficient
C_l	lift coefficient
C_m	pitching moment coefficient
\mathbf{f}, \mathbf{h}	vector functions
$\mathbf{f}_g, \mathbf{g}_g$	functions linking mesh positions and speeds to input vector
h	heave displacement
$\tilde{\mathbf{H}}_k$	discrete Markov parameter
$\tilde{\mathbf{H}}_{ls}(k)$	block Hankel matrix
M	freestream Mach number
$\hat{\mathbf{n}}$	unit normal vector on surface
p	pressure
t	time
\mathbf{u}	input vector
U_∞	freestream speed
\mathbf{V}	unperturbed surface fluid velocity vector
\mathbf{V}_p	wall velocity of an equivalent inviscid, irrotational flow
v_2	wall normal surface velocity
\mathbf{x}	continuous state vector
\mathbf{x}_k	discrete state vector
\mathbf{x}_g	mesh position
\mathbf{y}	continuous output vector
\mathbf{y}_k^m	modified discrete output vector

Greek Symbol

α	pitch angle
γ	ratio of specific heats
δ	flap angle
κ	reduced frequency
ω	frequency

1.0 INTRODUCTION

Accurate fluid models for prediction of unsteady flow features for aeroelastic calculations require solution of the full unsteady non-linear Euler or Navier-Stokes equations. The

drawback of implementing such methods is the high number of degrees of freedom, coupled with the thousands of parameter variations that must be investigated, which makes them too computationally expensive for routine use in industry. Therefore historically simpler methods which are not able to predict all the features encountered in the flight regime of modern aircraft have been used e.g. Doublet Lattice Methods (DLMs). Recent research has therefore focussed on the application of Model Order Reduction (MOR) schemes to unsteady Computational Fluid Dynamics (CFD) codes as this approach offers a potential increase in accuracy over methods such as DLM.

The objective of MOR schemes is to produce a computationally efficient Reduced Order Model (ROM) from the Euler or Navier-Stokes system that captures the dominant dynamic behaviour of the full order system. Whilst MOR of the continuous time Euler or Navier-Stokes equations is possible, in most CFD implementations either a discrete time or discrete frequency domain is used. Thus in many cases a discrete time or frequency domain ROM is produced, which can be used in some cases to obtain a continuous time domain ROM. The term, reduced order modelling, is widely used and covers a large number of quite different methods. Reviews of the various approaches are available in Dowell and Hall⁽¹⁾ and Antoulas⁽²⁾, but are not covered here since this paper focuses purely on an improvement to one MOR method.

The focus of this paper is the Eigensystem Realisation System Algorithm (ERA) method for MOR^(3,5,6,7,8,9), which builds on the work of Kung⁽⁴⁾. This is an efficient approximately balanced method⁽⁸⁾ that can be applied to CFD with only minor modifications to the inputs and outputs of the code. The truncated responses to input pulses are then sufficient for the MOR process. However there is one important question that arises with this method, namely what is an appropriate size for the input pulse for a CFD code. As explained in⁽¹⁰⁾ poor pulse size specification can cause non-physical behaviour to arise during the CFD iterations causing the CFD code not to converge. Experience has shown that the maximum change in pressure usually occurs on the first time step of the CFD scheme and a new and efficient method based on piston theory for estimating this pressure change and hence sizing the input pulses for both Euler and Navier-Stokes codes is described here.

2.0 TIME-CONTINUOUS NONLINEAR AND LINEAR STATE-SPACE SYSTEMS

In this work, the unsteady Euler or RANS equations are solved using a standard Jameson cell-centred finite-volume scheme code^(11,12), that is modified to be time accurate and allows moving meshes^(13,14,15). After spatial discretisation the CFD equations for the motion about a non-linear baseline Euler or RANS solution can be written⁽¹⁰⁾ in non-linear state space form as:

$$\begin{aligned}\frac{d\mathbf{x}(t)}{dt} &= \mathbf{f}(t, \mathbf{x}(t), \mathbf{u}(t)), \\ \mathbf{y}(t) &= \mathbf{h}(t, \mathbf{x}(t), \mathbf{u}(t)),\end{aligned}\quad \dots(1)$$

where (\mathbf{u}) is the input vector, (\mathbf{x}) is the state vector and (\mathbf{y}) is the output vector, containing quantities of interest such as changes to force coefficients or surface pressures. For example,

for an aerofoil undergoing linearised perturbations in pitch ($\Delta\alpha$), heave (Δh) and flap ($\Delta\delta$) motions; where the outputs of interest are the changes to the integrated coefficients of lift (ΔC_l), drag (ΔC_d), pitching moment (ΔC_m) and flap hinge moment (ΔC_h) compared to the initial mean values obtained from the steady nonlinear CFD solver then

$$\begin{aligned}\mathbf{u} &= \left[\Delta\alpha, \Delta\dot{\alpha}, \Delta h, \Delta\dot{h}, \Delta\delta, \Delta\dot{\delta} \right]^T, \\ \mathbf{y} &= \left[\Delta C_l, \Delta C_d, \Delta C_m, \Delta C_h \right]^T.\end{aligned}\quad \dots (2)$$

It should be noted here that the use of moving meshes with ERA is straightforward since the mesh positions \mathbf{x}_g and mesh speeds $\dot{\mathbf{x}}_g$ that arise in the differential equations are functions of the inputs:

$$\begin{aligned}\mathbf{x}_g &= \mathbf{f}_g(\mathbf{u}(t)), \\ \dot{\mathbf{x}}_g &= \mathbf{g}_g(\mathbf{u}(t)).\end{aligned}\quad \dots (3)$$

$$\dots (4)$$

Hence the mesh positions and speeds do not appear explicitly in the function \mathbf{f} in equation (1) as they can be written in terms of \mathbf{u} .

If the dynamic behaviour of the non-linear Euler or Navier-Stokes system (1) about the non-linear mean or steady flow solution is approximately linear then the non-linear system can be approximated by a linear time-continuous state-space system given by:

$$\begin{aligned}\frac{d\mathbf{x}(t)}{dt} &= \mathbf{A}\mathbf{x}(t) + \mathbf{B}\mathbf{u}(t), \\ \mathbf{y}(t) &= \mathbf{C}\mathbf{x}(t) + \mathbf{D}\mathbf{u}(t),\end{aligned}\quad \dots (5)$$

where the system matrices \mathbf{A} , \mathbf{B} , \mathbf{C} and \mathbf{D} are independent of time⁽¹⁶⁾. The linear responses of the unsteady CFD form the basis for the ERA approach. The linear responses are found either directly by linearising the CFD code⁽¹⁷⁾ so the system is truly linear (though it may not be written in the form (5)) or as the linear part of a non-linear response, which requires two non-linear unsteady simulations to be calculated^(5,16).

3.0 DISCRETE LINEAR STATE-SPACE SYSTEM

The CFD code used in this work is actually implemented in the discrete time domain and hence MOR is implemented to obtain a discrete-time ROM. In order to obtain the terms needed by the ERA algorithm to build a discrete ROM directly from the output responses without further manipulation⁽¹⁸⁾, a first order implicit finite difference scheme is used for the time derivative in (5) to give the discrete linear system⁽¹⁶⁾:

$$\begin{aligned}\mathbf{x}_k &= \tilde{\mathbf{A}}\mathbf{x}_{k-1} + \tilde{\mathbf{B}}\mathbf{u}_k, \\ \mathbf{y}_k^m &= \tilde{\mathbf{C}}\mathbf{x}_k,\end{aligned}\quad \dots (6)$$

where the subscript k denotes the value of a quantity at time level $k\Delta t$ and the discrete system output has been modified to $\mathbf{y}_k^m = \mathbf{y}_k - \mathbf{D}\mathbf{u}_k$, since \mathbf{D} in the output equation is known

and small for most problems of interest. The discrete system time-step dependent matrices are as follows

$$\begin{aligned}\tilde{\mathbf{A}} &= (\mathbf{I} - \Delta t \mathbf{A})^{-1}, \\ \tilde{\mathbf{B}} &= (\mathbf{I} - \Delta t \mathbf{A})^{-1} \mathbf{B} \Delta t, \\ \tilde{\mathbf{C}} &= \mathbf{C}.\end{aligned}$$

It should be noted that the corresponding continuous system output is then modified to be $\mathbf{y}^m(t) = \mathbf{y}(t) - \mathbf{D}\mathbf{u}(t)$. Further, it is important to emphasise that the first order discretisation should be seen as a low pass filter, as it highly damps high frequency terms allowing the easier identification of the usually more important low frequency terms in the discrete ROM. It should be noted that the discrete ROM is for a fixed time step; this is acceptable for many applications. However, if for example the ROM is to be used within a continuation algorithm⁽¹⁹⁾ then the time step must be able to vary. The discrete ROM is mapped back to the continuous space by inverting the transformation (7). The continuous time ROM produced from the discrete ROM can be put into discrete form with a different time step and using any finite difference approximation; hence the resulting ROM is not fixed as first order in time.

4.0 EXPLANATION OF ROLE OF PULSE RESPONSES WITHIN ERA

A discrete reduced order system is obtained from (6) using the ERA method^(4,3). ERA requires terms of the form

$$\tilde{\mathbf{H}}_k = \tilde{\mathbf{C}} \tilde{\mathbf{A}}^k \tilde{\mathbf{B}}, \quad \dots (7)$$

to be identified for $k \geq 0$. These terms are equal to the Markov parameters $\tilde{\mathbf{H}}_k$ of (6). The matrices $\tilde{\mathbf{H}}_k$ can be directly constructed as each column is the output response to a *unit* sample pulse input on one of the system inputs separately^(20,16). Once these terms are known the $l \times s$ block generalised Hankel matrix can written as:

$$\tilde{\mathbf{H}}_{ls}(k) = \begin{bmatrix} \tilde{\mathbf{H}}_k & \tilde{\mathbf{H}}_{k+1} & \tilde{\mathbf{H}}_{k+2} & \dots & \tilde{\mathbf{H}}_{k+s-1} \\ \tilde{\mathbf{H}}_{k+1} & \tilde{\mathbf{H}}_{k+2} & \tilde{\mathbf{H}}_{k+3} & \dots & \tilde{\mathbf{H}}_{k+s} \\ \cdot & \cdot & \cdot & & \cdot \\ \cdot & \cdot & \cdot & & \cdot \\ \cdot & \cdot & \cdot & & \cdot \\ \tilde{\mathbf{H}}_{k+l-1} & \tilde{\mathbf{H}}_{k+l} & \tilde{\mathbf{H}}_{k+l+1} & \dots & \tilde{\mathbf{H}}_{k+s+l-2} \end{bmatrix}. \quad \dots (8)$$

If it is assumed that the system has p outputs and m inputs then the Markov parameters will each have a size $p \times m$, hence the size of the Hankel matrix is $lp \times sm$. The parameters l and s must be chosen to ensure that enough terms are retained in the truncated responses. The partitioned singular value decomposition (SVD) for the Hankel matrix with $k = 0$ is given by

$$\tilde{\mathbf{H}}_{ls}(0) = \mathbf{U} \mathbf{\Sigma} \mathbf{V}^T, \quad \dots (9)$$

where $\mathbf{\Sigma}$ is an $sm \times sm$ diagonal matrix of singular values which are either positive or zero, with the singular values arranged in size order. The ERA process then determines the rank of the reduced order model of the system based on the number of elements of $\mathbf{\Sigma}$ which are larger

than some desired accuracy or by including only the r largest singular values in Σ , where r is prescribed. Then matrix $\tilde{\mathbf{H}}_{ls}(0)$ is partitioned and approximated⁽¹⁰⁾ as

$$\tilde{\mathbf{H}}_{ls}(0) \approx \mathbf{U}_r \Sigma_r \mathbf{V}_r^T, \quad \dots (10)$$

where unnecessary columns and rows of the matrices \mathbf{U} , Σ , \mathbf{V} have been deleted to reduce their size. The reduced matrix from \mathbf{U} is $\mathbf{U}_r : lp \times r$, the reduced matrix from Σ is $\Sigma_r : r \times r$ and the reduced matrix from \mathbf{V} is $\mathbf{V}_r : sm \times r$.

Then following⁽³⁾ it can be shown that one possible realisation of this reduced system is

$$\begin{aligned} \tilde{\mathbf{A}}_r &= \Sigma_r^{-1/2} \mathbf{U}_r^T \tilde{\mathbf{H}}_{rs}(1) \mathbf{V}_r \Sigma_r^{-1/2}, \\ \tilde{\mathbf{B}}_r &= \Sigma_r^{1/2} \mathbf{V}_r^T \mathbf{E}_m, \\ \tilde{\mathbf{C}}_r &= \mathbf{E}_p^T \mathbf{U}_r \Sigma_r^{1/2}, \end{aligned} \quad \dots (11)$$

where $\mathbf{E}_p = [\mathbf{I}_p, \mathbf{0}_p, \mathbf{0}_p, \dots, \mathbf{0}_p]$ has size $p \times lp$ and $\mathbf{E}_m^T = [\mathbf{I}_m, \mathbf{0}_m, \mathbf{0}_m, \dots, \mathbf{0}_m]$ has size $m \times sm$. This realisation $[\tilde{\mathbf{A}}_r, \tilde{\mathbf{B}}_r, \tilde{\mathbf{C}}_r]$ is not unique, because any non-singular matrix \mathbf{T} can be used to obtain another valid realisation $[\mathbf{T}\tilde{\mathbf{A}}_r\mathbf{T}^{-1}, \mathbf{T}\tilde{\mathbf{B}}_r, \tilde{\mathbf{C}}_r\mathbf{T}^{-1}]$.

The ERA method is implemented to obtain a discrete-time ROM of the CFD code, which is limited to the order of accuracy of the time-stepping scheme used in obtaining pulse responses and also to a fixed real time step. Consequently the discrete ROM cannot be accurately applied to problems involving structural models with discrete non-linearities (for example control surface freeplay) as the aerodynamic model could not capture the ‘‘switching’’ points between discrete regions⁽²¹⁾. This problem can lead to non-physical limit cycle behaviour arising in the solution⁽²²⁾. A time continuous ROM $[\mathbf{A}_r, \mathbf{B}_r, \mathbf{C}_r]$ does not have this restriction, since it can be solved for any time step size. The consistent method to obtain a continuous-time ROM is to invert the transformation used to obtain the discrete system matrices from the continuous system matrices⁽²³⁾.

Further it should be noted that the basic ERA scheme applied to short pulse response histories does not guarantee the stability of the resulting discrete-time ROM. A skilled user is usually able to specify a size of Hankel matrix and reduced model size to find a discretely stable scheme. There is a further stability issue in respect of continuous-time models obtained via the inverse of the first order implicit finite difference scheme, which means that not all stable discrete-time ROMs map to stable continuous-time ROMs. Recent work by Wales *et al*⁽¹⁸⁾ means that these stability issues can be overcome using an automated restarting approach.

5.0 PULSE INPUT SIZING

The sizing of the input pulses is a major consideration when using the ERA method for ROM generation. In most implementations this has been based on user experience gained via an expensive process of trial and error. Whilst inputting a *discrete unit sample pulse* on an input channel of a CFD code would directly output a column of the Markov parameter needed for ROM construction this can, for some input channels, lead to poorly converged solutions and in some cases solution breakdown. However, since the dynamic response of the system is approximated as linear (see equations (3) and (4)) a smaller input pulse can be used and the

output response scaled to give the response to a unit pulse and hence a column of the Markov parameter.

If the pulse size chosen is too large then during the solution process at each real-time step, the Euler and RANS equations may encounter non-physical solutions (before convergence is achieved). One area that this issue often arises is where there are supersonic velocities away from the aerofoil, which can lead to zero or negative pressures that prevent convergence and limiters fail to prevent this issue retarding convergence⁽¹⁰⁾. If the pulse size chosen is too small then the response may quickly approach the order of accuracy of the CFD scheme (maximum user specified residual) due to the exponential decay of the response.

The method for pulse sizing described here is based on piston theory (a tool more frequently used for supersonic and hypersonic aeroelastics) and is applicable to flows around subsonic and transonic aerofoils. The closed form of the piston theory equations yields a robust method of selecting a sample pulse size for ROM generation that overcomes the difficulties outlined above. This approach has minimal implementation costs and does not require any modification of the core CFD code.

5.1 Numerical Procedure

An *a priori* estimate of the response of the unsteady CFD about a baseline steady solution, can be found using the baseline pressure and velocity together with 1D piston theory, which considers a point on a moving surface as being analogous to a piston moving through a one dimensional channel^(25,26,27). Then using Bernoulli's equation and isentropic relations it can be shown that the pressure on the face of a one dimensional piston at the cell adjacent to the boundary is:

$$\frac{p_2}{p_1} = \left(1 + \frac{(\gamma - 1)}{2} \frac{v_2^2}{a_1^2} \right)^{\frac{2\gamma}{\gamma - 1}}, \quad \dots(12)$$

where subscripts 1 and 2 refer to a quantity before and after the perturbation respectively. p is the local static pressure, a is the local speed of sound, γ is the adiabatic index (assumed here to be 1.4) and v is the wall normal surface fluid velocity due to the perturbation. The wall normal surface fluid velocity v_2 can be described in terms of the surface normals as:

$$v_2 = \Delta \mathbf{V} \cdot \hat{\mathbf{n}}_2 + \mathbf{V} \cdot (\hat{\mathbf{n}}_2 - \hat{\mathbf{n}}_1), \quad \dots(13)$$

where $\hat{\mathbf{n}}$ is a unit normal vector on the body surface. \mathbf{V} is the unperturbed surface fluid velocity vector and $\Delta \mathbf{V}$ is the change in the surface fluid velocity vector due to the aerofoil motion, which in this case equals the prescribed surface velocity. Note that this formulation follows the approach of Zhang *et al*⁽²⁸⁾ who apply piston theory around the local pressure at each cell adjacent to the boundary, rather than the free stream conditions.

5.2 Extension to Viscous Flows

The extension of the piston theory approach to the RANS equations is complicated by the fact that the no slip boundary condition for a non porous wall means that $\mathbf{V} = 0$ and hence piston

theory (12) cannot be directly applied. Instead, the velocity \mathbf{V}_P at the wall of an equivalent inviscid, irrotational flow is approximated by assuming that a surface bounding streamline exists and that the pressure distribution is that of the viscous flow wall boundary. Then using simple Bernoulli's equation (but allowing density to change) gives:

$$|\mathbf{V}_P| = \sqrt{\frac{2(p_\infty - p_B)}{\rho_B} + \frac{\rho_\infty}{\rho_B} (\mathbf{V}_\infty)^2},$$

where p_B, ρ_B are the prescribed pressures and densities at the boundary of the viscous wall and p_∞, ρ_∞ are the free stream pressures and densities. The velocity vector \mathbf{V}_P becomes:

$$\mathbf{V}_P = \hat{\mathbf{S}}\mathbf{L} \cdot |\mathbf{V}_P|,$$

where $\hat{\mathbf{S}}\mathbf{L}$ is the unit direction vector of the equivalent surface bound streamline.

5.3 Time Step Size

One dimensional piston theory has been shown to give good results for periodic pitching so long as any of the conditions (14), (15) and (16) below are true^(25,29).

$$M^2 \gg 1, \quad \dots(14)$$

$$\kappa M^2 \gg 1, \quad \dots(15)$$

$$\kappa^2 M^2 \gg 1, \quad \dots(16)$$

where M is the freestream Mach number and $\kappa = \omega \cdot c / U_\infty$ is a non-dimensional reduced frequency. Here ω is the circular frequency, c is the chord and U_∞ is the freestream speed. Within the context of the subsonic high frequency oscillation condition (16) becomes:

$$\left(\frac{\omega \cdot c \cdot M}{U_\infty} \right)^2 \gg 1. \quad \dots(17)$$

For the pulse response however, there is no circular frequency condition. For the pulse estimations used here, the circular frequency ω is replaced with $\frac{1}{\Delta t}$. Consequently, the piston approximation for pulse sizing is expected to give best results when

$$\left(\frac{c \cdot M}{U_\infty \cdot \Delta t} \right)^2 \gg 1. \quad \dots(18)$$

In this research, it has been found that this condition is adequate and that while piston theory is traditionally only valid at very high Mach numbers or very high frequencies, for subsonic pulse responses the time step which satisfies (18) may be significantly larger than the time step required to resolve the high frequencies required to satisfy (16).

5.4 Results of Input Sizing Tests

5.4.1 2D Euler Results

The accuracy of the pressure predicted by piston theory on the first time step directly after a pulse is tested by comparing to non-linear Euler simulations for three test cases. Only results

from the first time step are considered as the instantaneous response produced by a sample pulse input at this time has been found to be the key factor in ensuring: that solutions do not encounter non-physical behaviour which prevents convergence and that the pulse is large enough to ensure a response beyond the accuracy specified for the CFD code. The test cases all use the NACA0012 aerofoil with a 25% flap, which can undergo heave and pitch (about quarter chord) motions. The mesh used has 139x15 cells (Figure 1) and the flow solver is an implicit cell centred finite volume dual time Euler scheme based on the standard Jameson scheme. The mean flow solutions for the inviscid test cases are shown in Figure 2.

The velocity expansion (13) can be expressed for the pulse inputs as:

$$v_2 = \begin{cases} \mathbf{V} \cdot (\hat{\mathbf{n}}_2 - \hat{\mathbf{n}}_1) & \bar{\Delta}\alpha \text{ Pitch pulse} \\ (\mathbf{a} - \mathbf{a}_x) \dot{\alpha} \cdot \hat{\mathbf{n}}_2 & \bar{\Delta}\dot{\alpha} \text{ Pitch rate pulse,} \\ 0 & \bar{\Delta}h \text{ Heave pulse,} \\ \mathbf{h} \cdot \hat{\mathbf{n}}_2 & \bar{\Delta}\dot{h} \text{ Heave rate pulse,} \\ \mathbf{V} \cdot (\hat{\mathbf{n}}_2 - \hat{\mathbf{n}}_1) & \bar{\Delta}\delta \text{ Flap Pulse,} \\ (\mathbf{b} - \mathbf{b}_x) \dot{\delta} \cdot \hat{\mathbf{n}}_2 & \bar{\Delta}\dot{\delta} \text{ Flap rate pulse .} \end{cases} \quad \dots (19)$$

The component of normal velocity in the expansion for heave displacement is predicted to be zero as the normals do not change. The results in the following sections will show that the nonlinear response to a pure heave displacement, although non zero, remains very small.

Tables 1 and 2 give an overview of the steady flow conditions and pulse sizes used in the test cases. In Table 1 a baseline set of pulse input sizes is defined as $scale=1$. These pulse size values are then scaled by a factor $scale=5^n$ to allow a simple rescaling of the results to check for linearity.

The unsteady pulse responses (Figures 3-8) are shown as a change in pressure and integral force from the nonlinear mean solution

$$\bar{\Delta}p = p_2 - p_1, \quad \dots (20)$$

$$\bar{\Delta}C_F = [C_F]_2 - [C_F]_1, \quad \dots (21)$$

where p is the non-dimensional static pressure and C_F is the respective integral force coefficient ($F = L, M, H$ for lift, pitching moment and hinge moment). Again, subscripts 1 and 2 represent the values before and after the first time step when the pulse is applied. The pressure change results are shown for the four different pulse sizes (from Table 1), with the values rescaled using $scale$ to demonstrate the approximate linearity of the response.

In interpreting the results the key measures are:

1. The maximum pressure change predicted by piston theory for unit input should be of the same order of magnitude as the maximum pressure change from CFD scaled for unit pulse input. It should be noted that precise accuracy is not required as piston theory is only being used to select a pulse size.
2. The change in integral force coefficients predicted by piston theory should also have a similar order of magnitude to the CFD values for the same size of input. Again precise accuracy is not required.

This is discussed further in Section 6.

For test case 1, $\kappa^2 M^2 = 16$ which is much greater than 1; for test case 2 $\kappa^2 M^2$ is close to the limiting value of 1 and for test case 3 the criteria for $\kappa^2 M^2$ is violated. For test cases 1 and 2 the initial integral values for lift and pitching moment are accurately predicted by the piston theory. As can be seen from the pressure responses, the piston theory cannot capture the merging of the trailing edge pressure with the wake and hence hinge moment coefficients are less accurately predicted. Test case 3 is run at an unrealistically high time step which would not normally be encountered for aeroelastic simulations. However even here (case 3) the correct order of magnitude of the integral forces and the maximum/minimum surface pressures is captured by piston theory. The largest pulse size ($scale = 125$) is selected to be unfavourably large. Many of the responses for the large pulse inputs are seen to be nonlinear. For test case 3, the responses to pitch (α) and heave rate (\dot{h}) include the influence of shock waves which were not present in the steady flow. In general these large pulse inputs struggled with convergence and were accompanied by very large changes in the integral force values.

Table 1
Pulse Inputs

Pulse	[units]	scale = 1	scale = 5	scale = 25	scale = 125
$\bar{\Delta}\alpha$	deg	0.08	0.4	2	10
$\bar{\Delta}\dot{\alpha}$	deg/s	0.4	2	10	50
$\bar{\Delta}h$	c	0.001	0.005	0.025	0.125
$\bar{\Delta}\dot{h}$	c/s	0.008	0.04	0.2	1.0
$\bar{\Delta}\delta$	deg	0.08	0.4	2	10
$\bar{\Delta}\dot{\delta}$	deg/s	0.4	2	10	50

Table 2
Test Cases

Case	α_0	M	Δt_{REAL}	$\kappa^2 M^2$
1	0.0	0.8	0.2	16
2	2.0	0.3	0.2	2.25
3	0.0	0.7	2.0	0.1225

5.4.2 2D Viscous Results

As for the Euler simulations of the previous section, the pressure and the integrated forces for the first time step directly after the pulse is compared with the piston theory. The test cases used are as described for the Euler simulations with the addition that the Reynolds number for all cases is 1×10^7 . The mesh and steady flow solution are shown in Figures 9 and 10 for the RANS solver.

The results for the RANS/piston comparisons are shown in Figures 11 to 16. Unlike the Euler comparisons, where the pressure distribution was still well predicted for Case 2, the piston theory only produces accurate pressure distributions for case 1 where condition (18) is valid. However the accuracy of the integrated coefficients is still excellent, even for the hinge moment if it is remembered that only an order of magnitude analysis is required.

6.0 PRACTICAL APPLICATION

When running CFD codes to obtain the pulse responses needed for ERA ROM generation, piston theory is applied to size the pulses to avoid convergence issues. The following work flow process is applied:

1. Generate nonlinear mean flow solution
2. Apply local one-dimensional piston theory using equation (12) to find the change in force coefficients from the mean values for a unit pulse input.
 - (a) The required pulse size to achieve a prescribed integral force change $\Delta\overline{C}_F$ is achieved by scaling the linear integral force change from the piston theory. The resulting scaling factor defines the pulse input magnitude for the CFD solver.
 - (b) Check that equation (12) does not predict very low or negative surface pressures for the rescaled pulse size.
3. Check the mesh integrity when deformed for pulse input of the size determined in step 2.
4. Apply the pulse input to the CFD solver.
5. Check the final response is as expected and fully captured within the accuracy of the converged solution.

It should be noted that the prescribed integral force change $\Delta\overline{C}_F$ depends heavily on the precision of the output and the control the user has over it. One of the main advantages of using an ERA based ROM is that little or no change to the CFD code is required, however this means that the accuracy constraints of the output files of the code may be fixed and varies from code to code. Further if the output forces are not the change from mean values, but absolute values then the accuracy is also impacted by the relative ratio of the change in force coefficients to the mean force coefficient values. Thus absolute guidelines are not possible as it will depend on the specific application.

7.0 CONCLUSIONS

The work described here has found that prescribing a required change in the integral forces and using piston theory to estimate the required pulse size for the Euler and RANS equations in most cases leads to an appropriate pulse size. However for robustness: the pressures are checked to ensure low or negative values are avoided, and if appropriate, the size of the pulse is reduced and the displaced mesh integrity for the maximum pulse displacements is checked before simulations are commenced. It has been found that for our CFD code prescribed values of $\Delta\overline{C}_F = 0.01 \dots 0.1$ (for $F=L, M, H$) are suitable for most cases depending on the steady state pressure distribution. For the case of the heave pulse sizing, where piston theory gives a zero response, an amplitude of $h = O(0.01c)$ has been found to be suitable for all cases considered.

8.0 ACKNOWLEDGEMENTS

The authors would like to acknowledge EPSRC, who funded this work.

REFERENCES

1. DOWELL, E.H. and HALL, K.C., Modelling of fluid-structure interaction, *Annual Rev. Fluid Mech.*, 2001, **33**, pp445-490.
2. ANTOULAS, A.C., Approximation of large-scale dynamical systems, 2005, *Advances in Design and Control*, SIAM.
3. JUANG, J.-N. and PAPPAS, R.S., An eigensystem realization algorithm for modal parameter identification and model reduction. *Journal of Guidance, Control and Dynamics*, 1985, **8**, (5), pp620-627.
4. KUNG, S.-Y., A new identification and model reduction algorithm via singular value decomposition, 1978, *Proceedings of the 12th Asilomar conference on circuits, systems and computers*.
5. SILVA, W.A., Discrete-time linear and nonlinear aerodynamic impulse responses for efficient CFD analyses. Ph.D. Thesis, Department of Applied Science, College of William and Mary, Virginia, USA, 1997.
6. SILVA, W.A. and RAVEH, D.E., Development of Unsteady Aerodynamic State-Space Models from CFD-Based Pulse Responses, 2001, *42nd AIAA/ASME/ASCE/AHS/ASC Structures, Structural Dynamics and Materials Conference*, Paper No AIAA-2001-1213.
7. GAITONDE, A.L. and JONES, D.P., Reduced order state-space models from the pulse responses of a linearised CFD scheme, *Int J. Numer. Meth. Fluids*, 2003, **42**, pp581-606.
8. MA, Z., AHUJA, S. and ROWLEY, C., Reduced order models for control of fluids using the Eigensystem Realization Algorithm, *Theor. Comput. Fluid Dyn.*, 2011, **25** pp233-247.
9. WALES, C.J., GAITONDE, A.L. and JONES, D.P., Stabilisation of Reduced Order Models via Restarting, *Int. J. Numer. Meth. Fluids*, 2013, **83**, pp578-599.
10. GRIFFITHS, L., Reduced order model updating, PhD Thesis, University of Bristol, 2014.
11. JAMESON, A., SCHMIDT, W. and TURKEL, E., Numerical solution of the Euler equations by finite volume method using Runge-Kutta time-stepping schemes, 1981, *AIAA 14th Fluid and Plasma Dynamic Conference*, Paper No AIAA-1981-1259.
12. KROLL, N. and JAIN, R.K., Solution of two-dimensional Euler equations - Experience with a finite volume code, 1987, *Forschungsbericht, DFVLR-FB 87-41*, Braunschweig, Germany.
13. GAITONDE, A.L., A dual time method for the solution of the unsteady Euler equations, *Aeronautical Journal*, 1994, **98**, No 978.
14. JAMESON, A.J., Time dependent calculations using multigrid, with applications to unsteady flows past airfoils and wings, Paper No AIAA-91-1596 1991.
15. ARNONE, A., LIOU, M.S. and POVINELLI, L., Integration of Navier-Stokes equations using dual time stepping and a multigrid method, *AIAA Journal*, 1995, **33**.
16. GAITONDE, A.L. and JONES, D.P., Study of linear response identification techniques and reduced order model generation for a 2D CFD scheme, *Int. J. Numer. Meth. Fluids*, 2006,

- 52, No 12, pp1361-1402.
17. GAITONDE, A.L. and JONES, D.P., Solutions of the 2D linearised unsteady Euler equations on moving meshes, *Proceedings of the Institution of Mechanical Engineering*, 2002, **216**, Part G, Journal of Aerospace Engineering, pp89-104.
 18. WALES, C., GAITONDE, A.L. and JONES, D.P., Stabilisation of Reduced Order Models via Restarting. *Int. J. Numer. Meth. Fluids*, 2013, **73**, No 6, pp78-599.
 19. JONES, D., ROBERTS, I. and GAITONDE, A., Identification of limit-cycles for piecewise non-linear aeroelastic systems, *Journal of Fluids and Structures*, 2007, **23**, No 7.
 20. APLEVICH, J.D., The essentials of linear state-space systems, 2000, Wiley.
 21. CONNER, M., VIRGIN, L. and DOWELL, E., Accurate numerical integration of state-space models for aeroelastic systems with freeplay, *AIAA Journal*, 1996, **34**, pp2202-2205.
 22. LIN, W. and CHENG, W., Nonlinear flutter of loaded lifted surfaces (i) & (ii), *Journal of the Chinese Society of Mechanical Engineers*, 1993, **14**, pp446-466.
 23. GAITONDE, A.L. and JONES, D.P., Calculations with ERA based reduced order aerodynamic models, 2006, *AIAA 24th Applied Aerodynamics Conference*, Paper No AIAA-2006-2999.
 24. GRIFFITHS, L., JONES, D. and FRISWELL, M., Pulse sizing for constructing reduced order models of the Euler equations, In International Forum on Aeroelasticity and Structural Dynamics conference, IFASD-2011-195, 2011.
 25. ASHLEY, H. and ZARTARIAN, G., Piston theory - a new aerodynamic tool for the aeroelastician, *Journal of the Aeronautical Sciences*, 1956, **23**, pp1109-1118.
 26. LIGHTHILL, M.J., Oscillating airfoils at high Mach number, *Journal of the Aeronautical Sciences*, 1953, **20**, No 6, pp402-406.
 27. VAN DYKE, M.D., Supersonic flow past oscillating airfoils including nonlinear thickness effects, 1953, *NACA Technical Note 2982*.
 28. ZHANG, W., YE, Z., ZHANG, C. and LIU, F., Supersonic Flutter Analysis Based on a Local Piston Theory, *AIAA Journal*, 2009, **47**, No 10, pp2321-2328.
 29. LANDAHL, M., MOLLO-CHRISTENSEN, E.L. and ASHLEY, H., Parametric Studies of Viscous and Nonviscous Unsteady Flows, 1955, *O.S.R. Technical Report 55-13*.

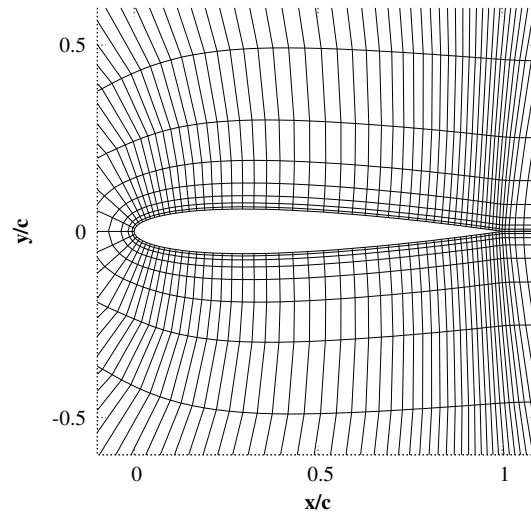


Figure 1. Finite volume Euler mesh used for all 2D Euler pulse sizing test cases (139x15 cells, 99 cells over the aerofoil)

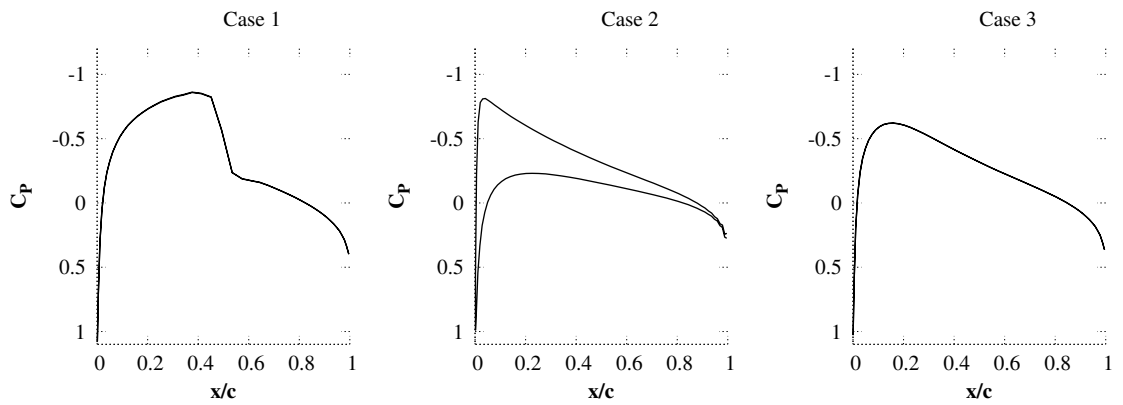


Figure 2. Nonlinear mean flow solutions

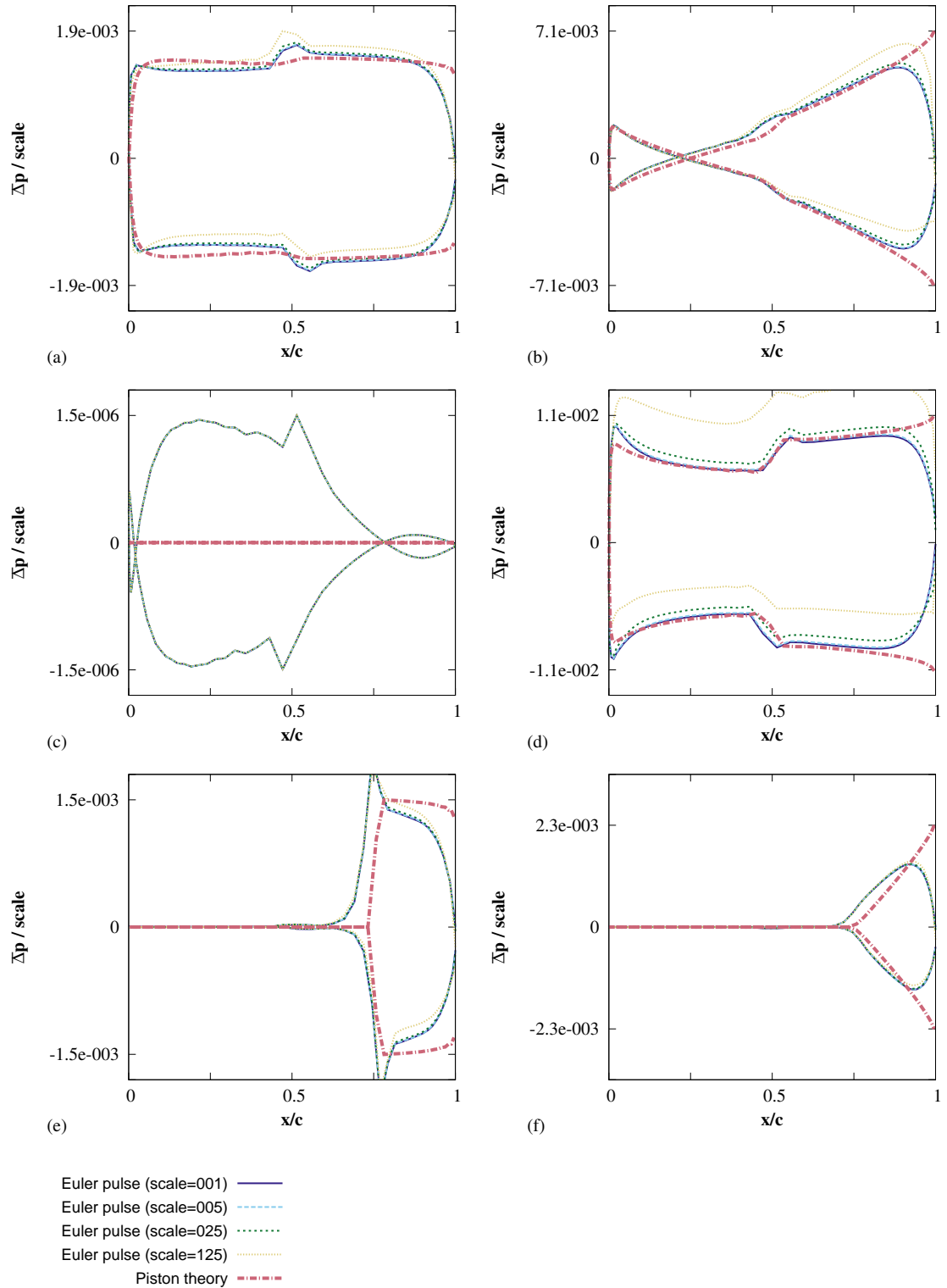


Figure 3. Test case 1 - Scaled pressure response $\bar{\Delta P}$, from Eqn 20 using the viscous wall condition. Responses are shown for (a) α ; (b) $\dot{\alpha}$; (c) h ; (d) \dot{h} ; (e) δ ; (f) $\dot{\delta}$, the pulse magnitudes are given in Table 1.

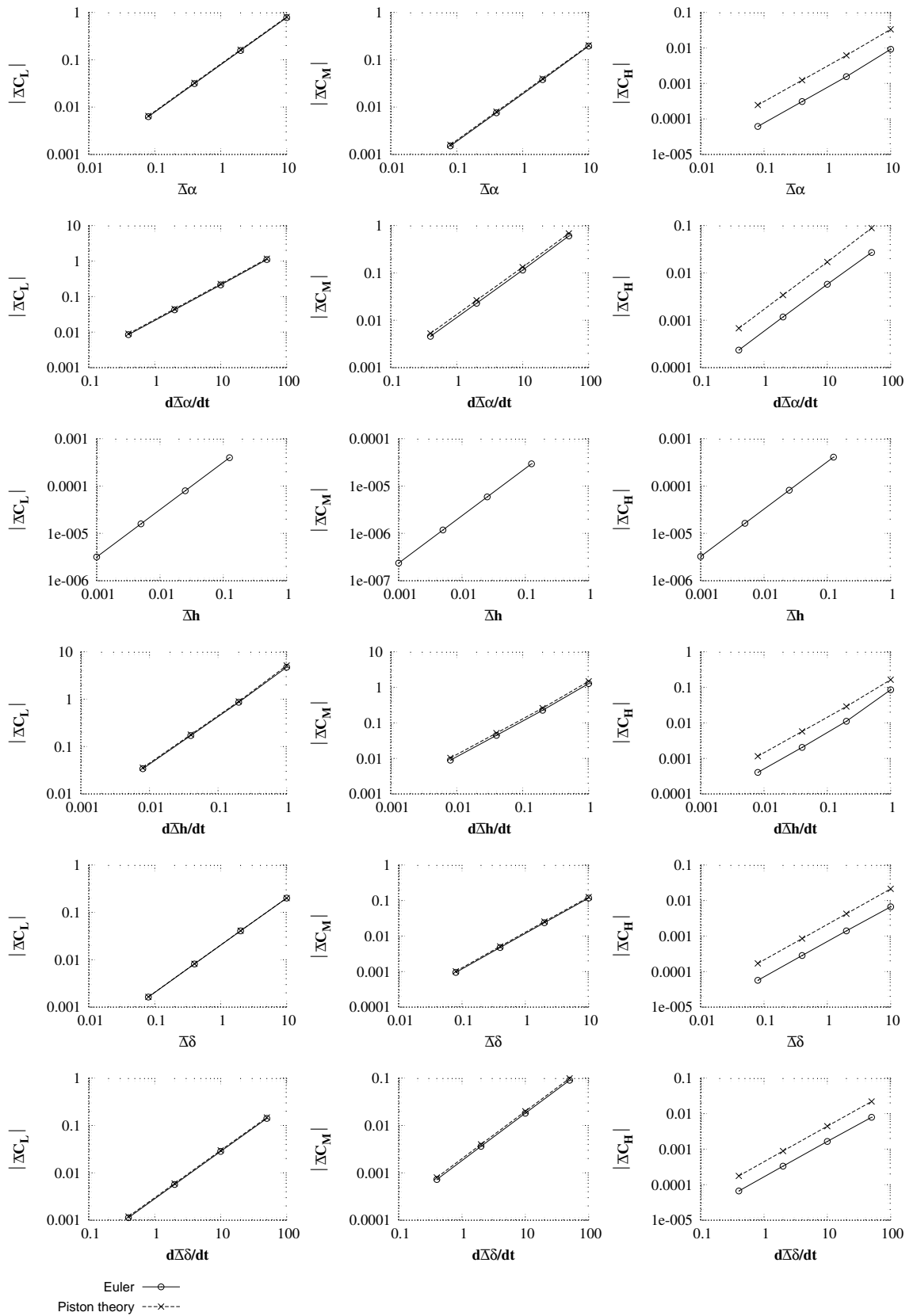


Figure 4. Test case 1 - Integral response (C_l, C_m, C_h). Each row corresponds to the pulse of a row in Table 1 and the points on each plot correspond to the four scales in Table 1

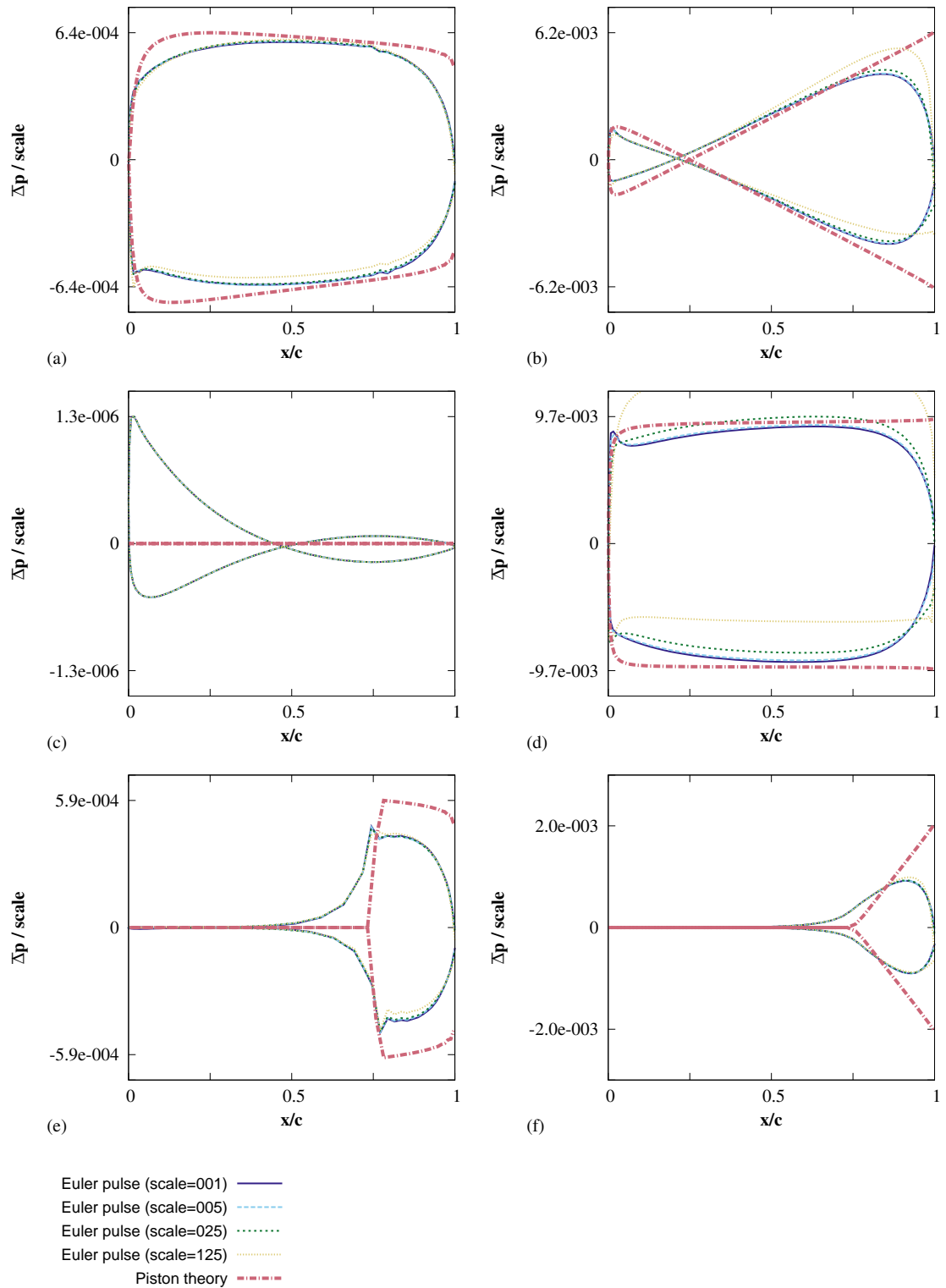


Figure 5. Test case 2 - Scaled pressure response $\bar{\Delta P}$, from Eqn 20 using the viscous wall condition. Responses are shown for (a) α ; (b) $\dot{\alpha}$; (c) h ; (d) \dot{h} ; (e) δ ; (f) $\dot{\delta}$, the pulse magnitudes are given in Table 1.

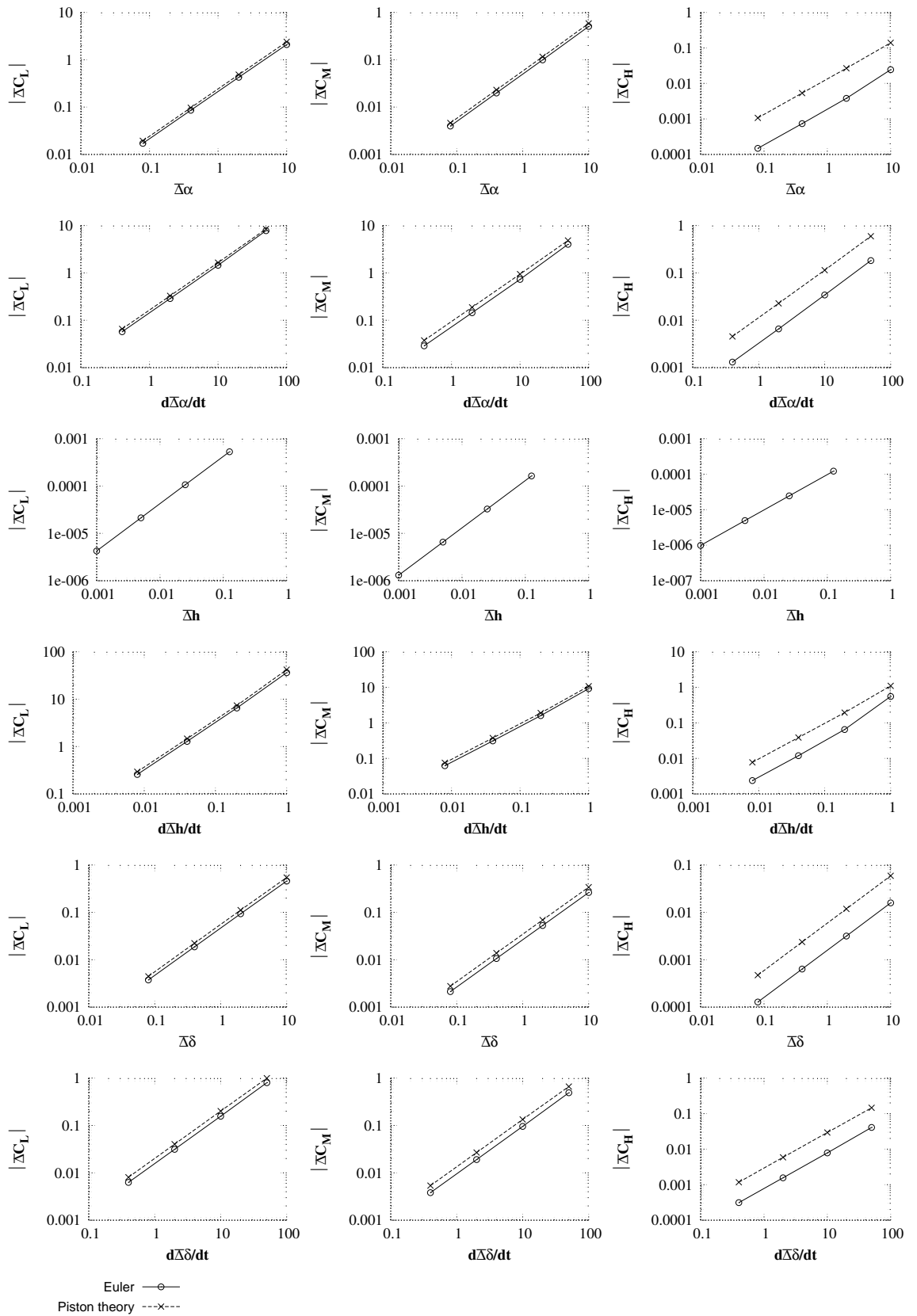


Figure 6. Test case 2 - Integral response (C_l, C_m, C_h). Each row corresponds to the pulse of a row in Table 1 and the points on each plot correspond to the four scales in Table 1

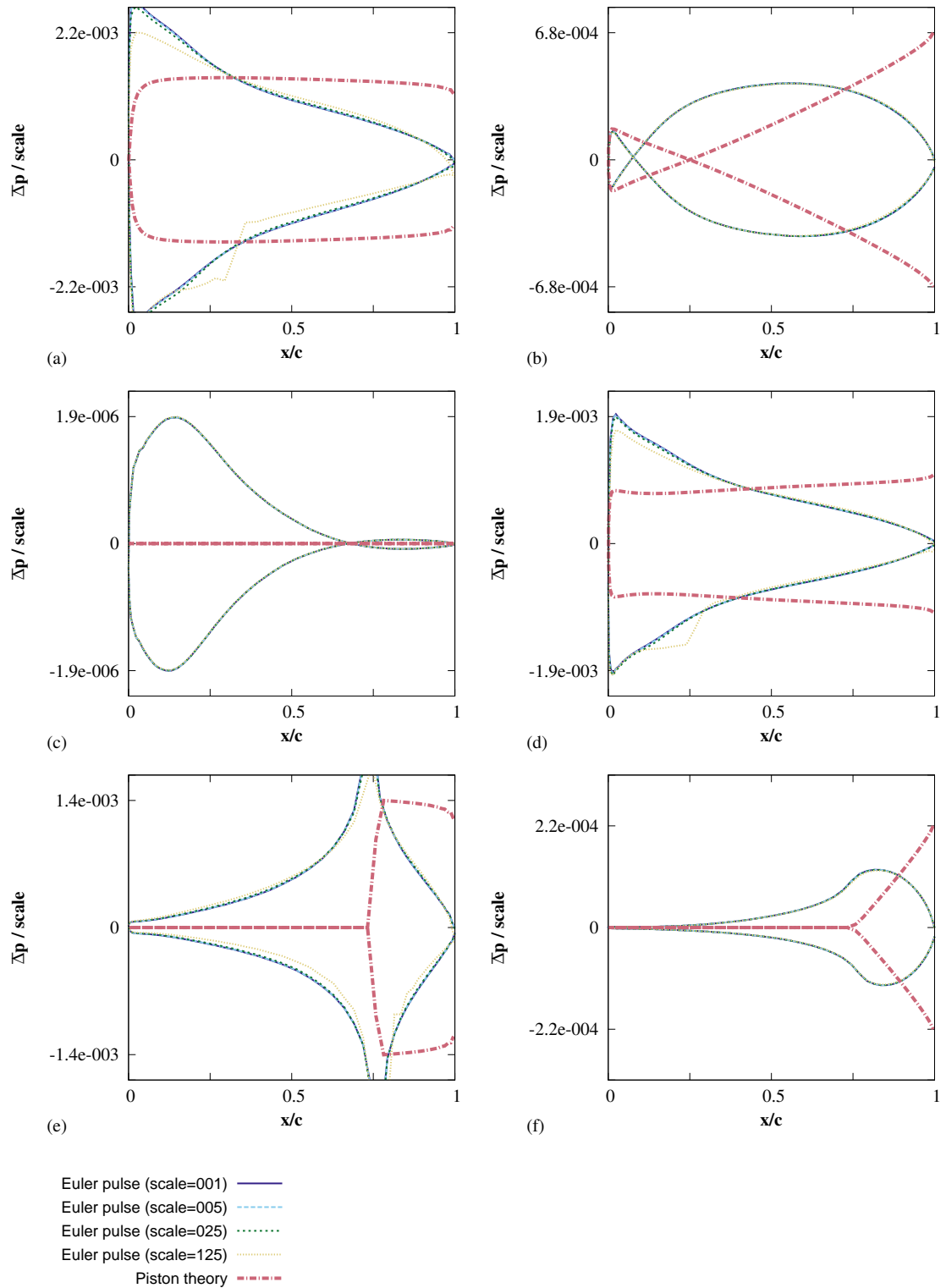


Figure 7. Test case 3 - Scaled pressure response $\bar{\Delta P}$, from Eqn 20 using the viscous wall condition. Responses are shown for (a) α ; (b) $\dot{\alpha}$; (c) h ; (d) \dot{h} ; (e) δ ; (f) $\dot{\delta}$, the pulse magnitudes are given in Table 1.

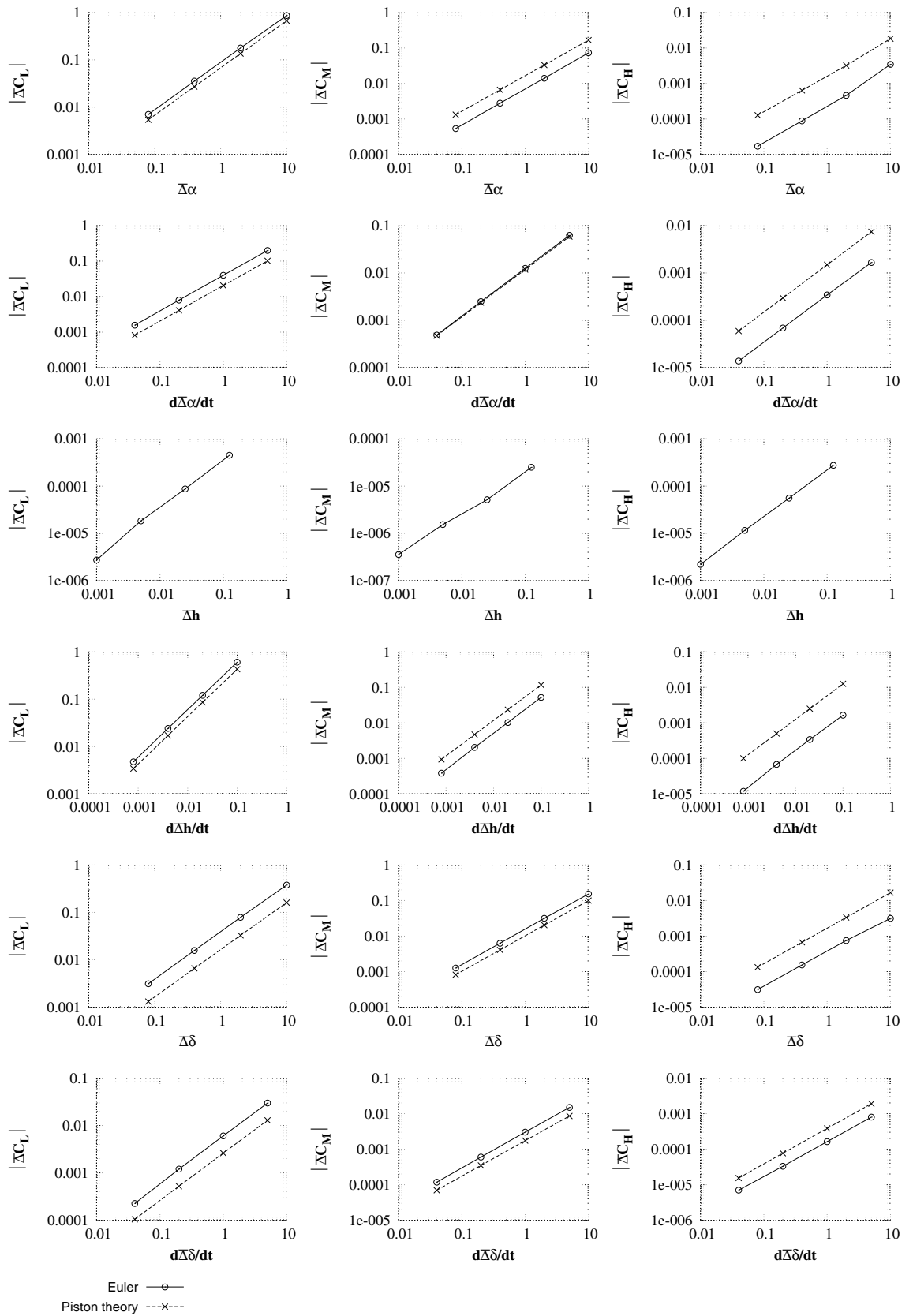


Figure 8. Test case 3 - Integral response (C_L, C_M, C_h). Each row corresponds to the pulse of a row in Table 1 and the points on each plot correspond to the four scales in Table 1

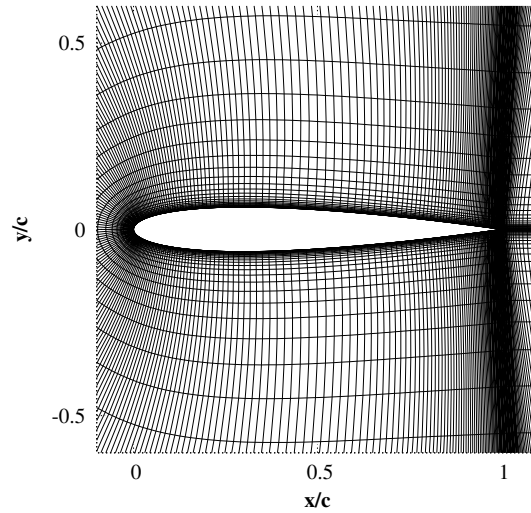


Figure 9. Finite volume Navier-Stokes mesh used for all 2D Navier-Stokes pulse sizing test cases (401x50 cells, 301 cells over the airfoil)

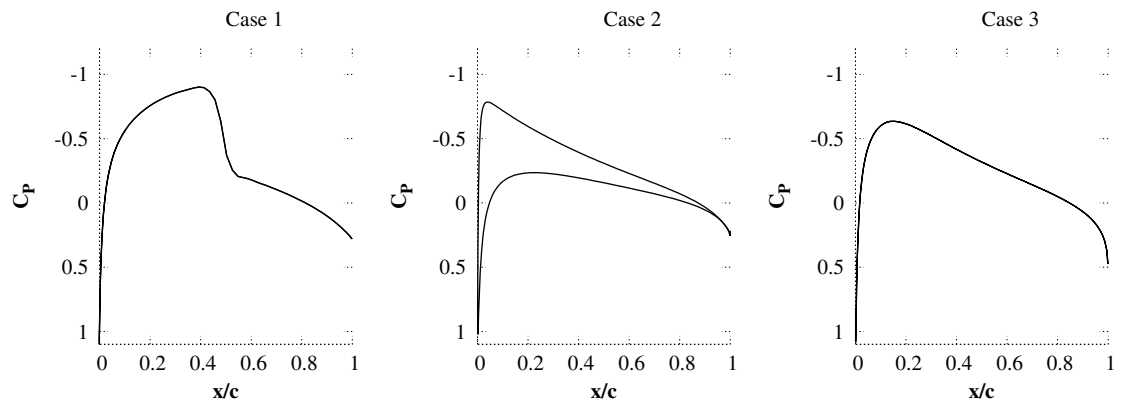


Figure 10. Nonlinear mean flow solutions

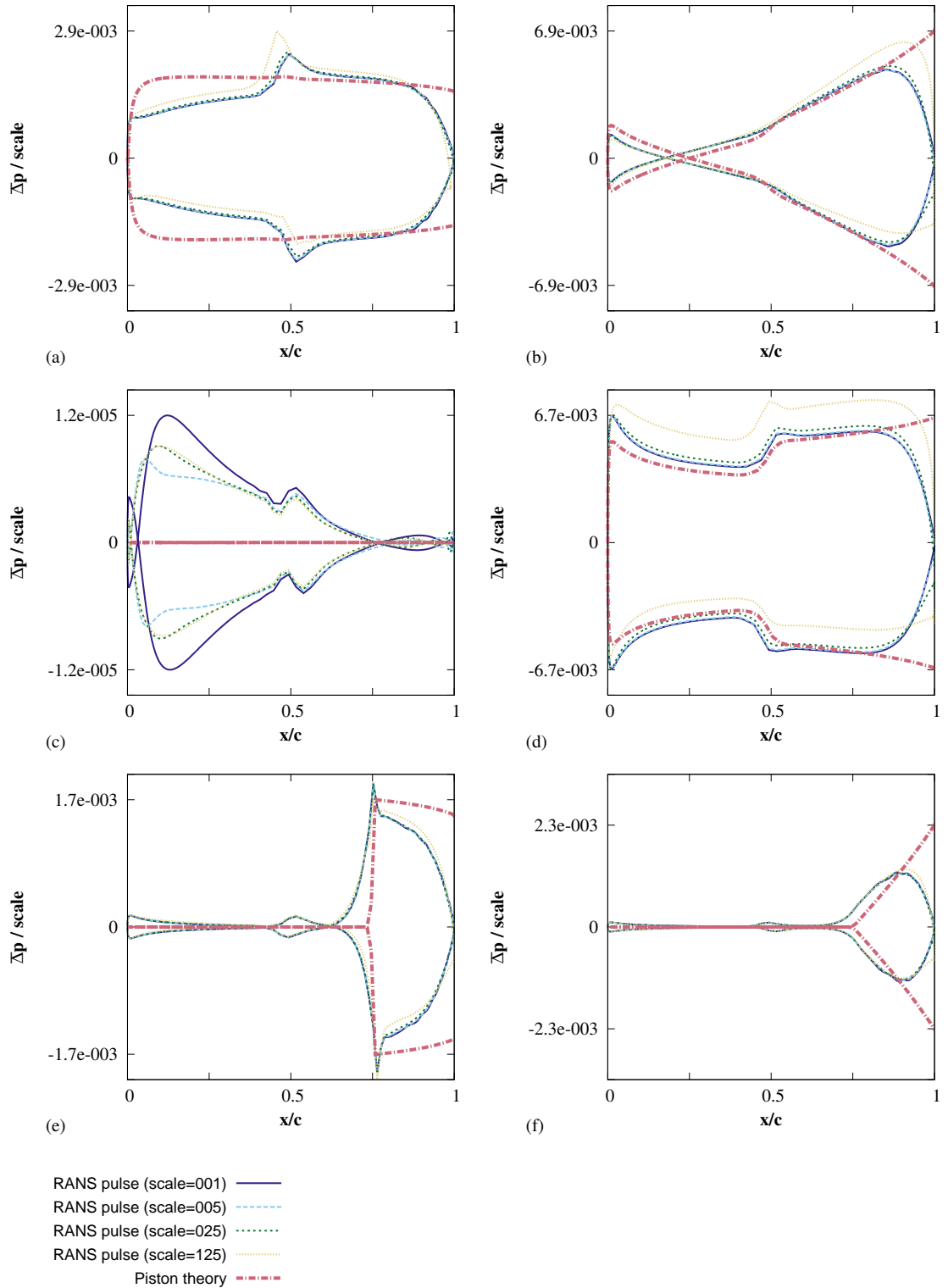


Figure 11. Test case 1 - Scaled pressure response $\bar{\Delta}P$, from Eqn 20 using the viscous wall condition. Responses are shown for (a) α ; (b) $\dot{\alpha}$; (c) h ; (d) \dot{h} ; (e) δ ; (f) $\dot{\delta}$, the pulse magnitudes are given in Table 1.

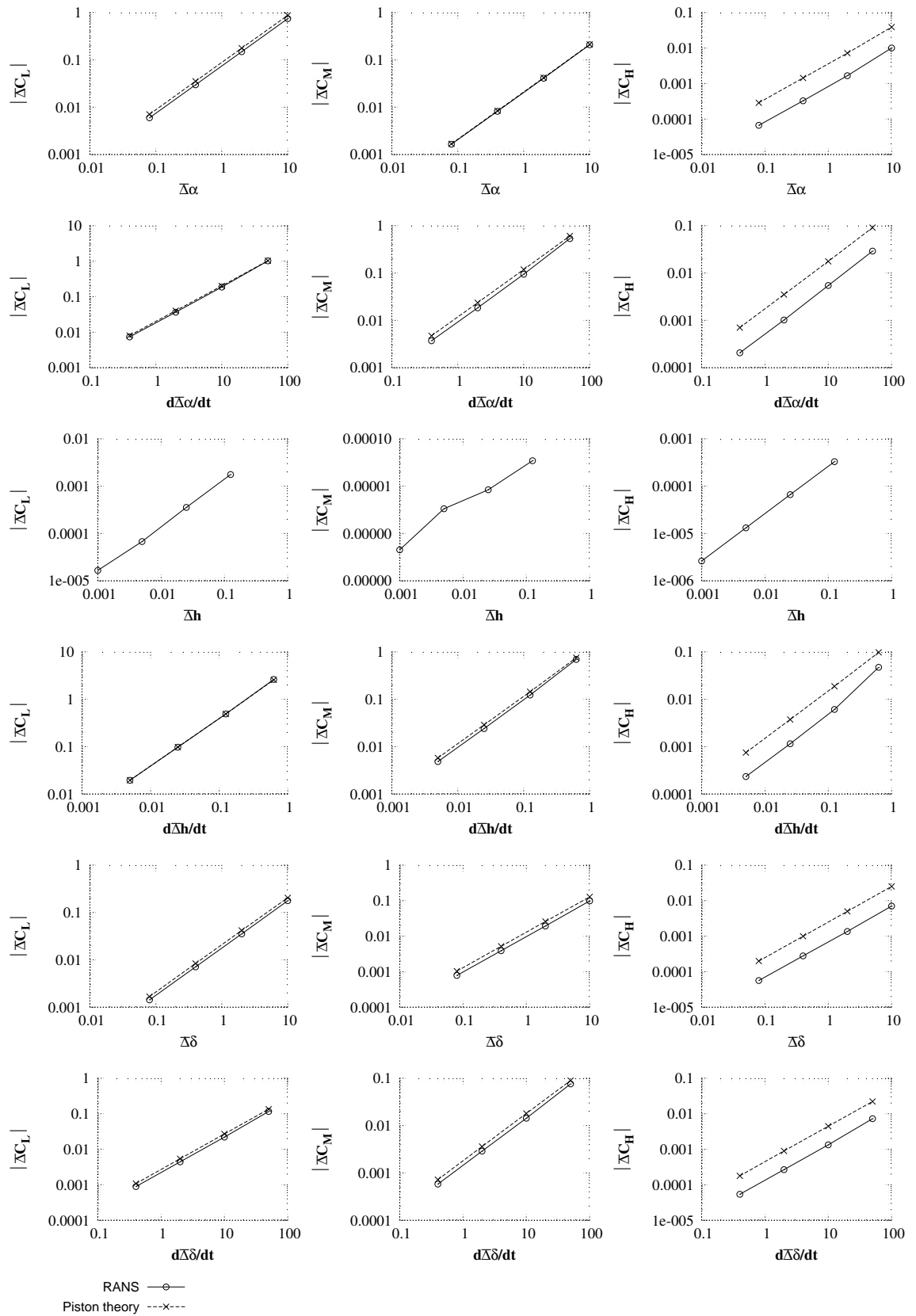


Figure 12. Test case 1 - Integral response (C_l, C_m, C_h). Each row corresponds to the pulse of a row in Table 1 and the points on each plot correspond to the four scales in Table 1

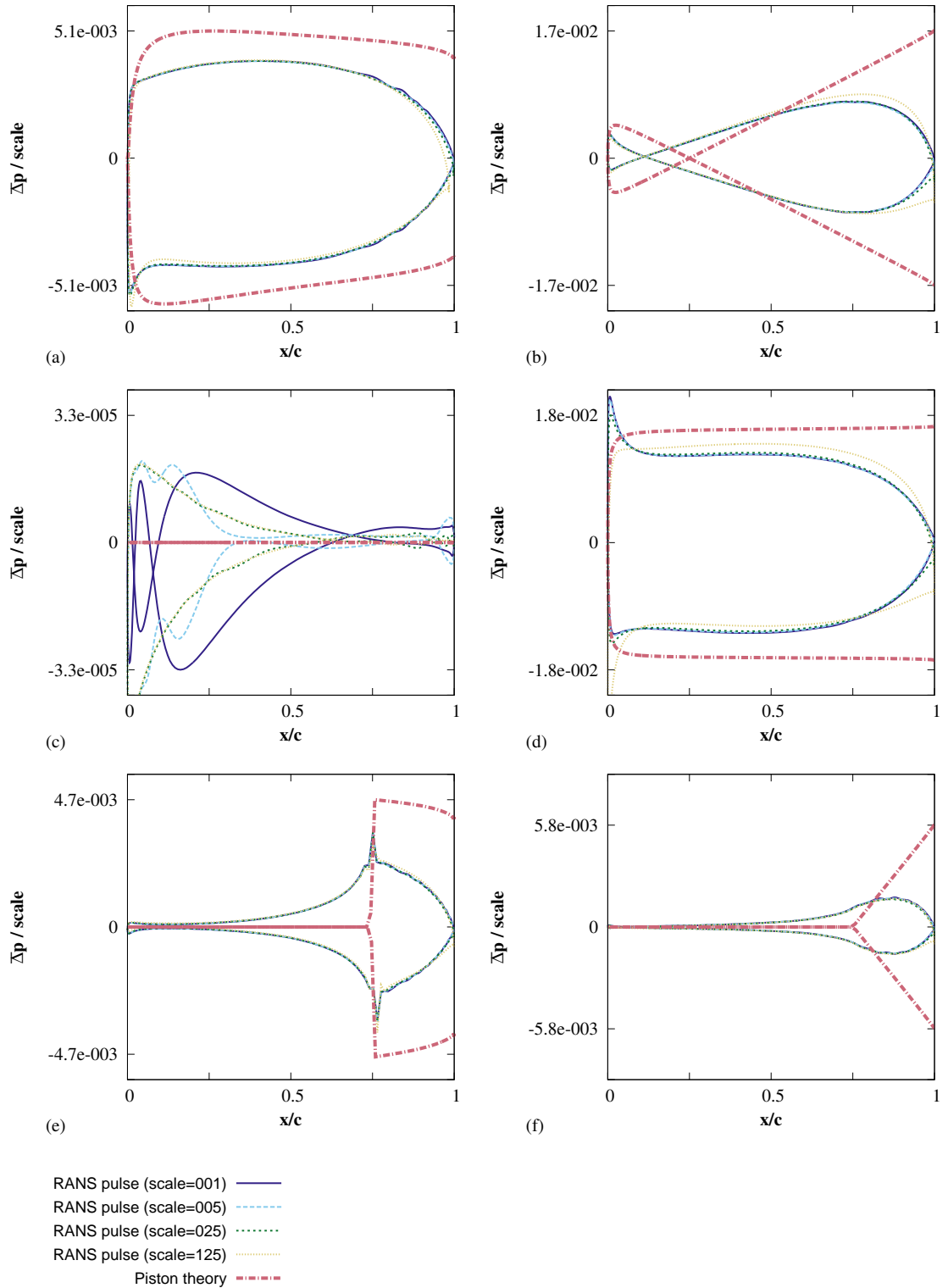


Figure 13. Test case 2 - Scaled pressure response $\bar{\Delta}P$, from Eqn 20 using the viscous wall condition. Responses are shown for (a) α ; (b) $\dot{\alpha}$; (c) h ; (d) \dot{h} ; (e) δ ; (f) $\dot{\delta}$, the pulse magnitudes are given in Table 1.

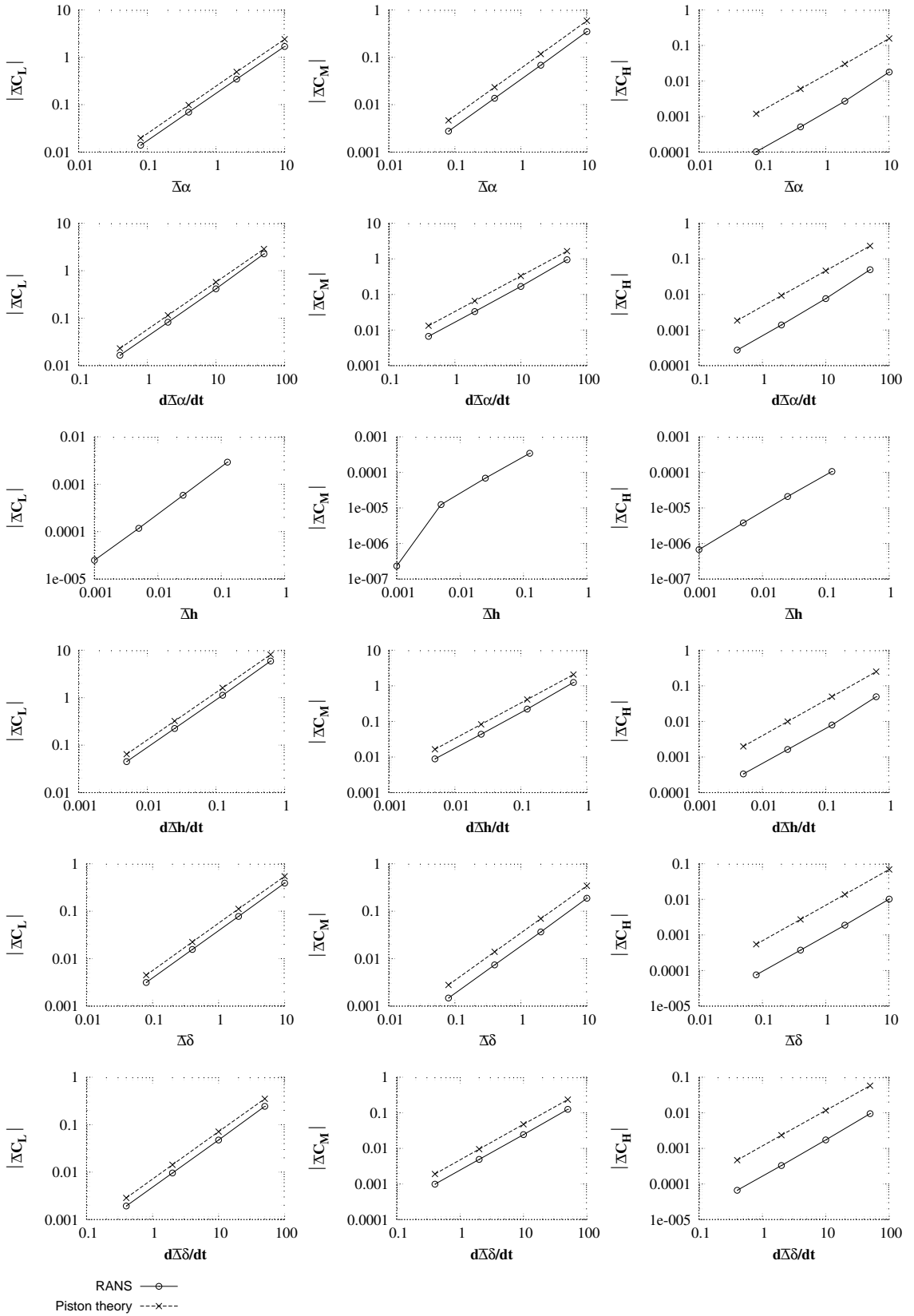


Figure 14. Test case 2 - Integral response (C_l, C_m, C_h). Each row corresponds to the pulse of a row in Table 1 and the points on each plot correspond to the four scales in Table 1

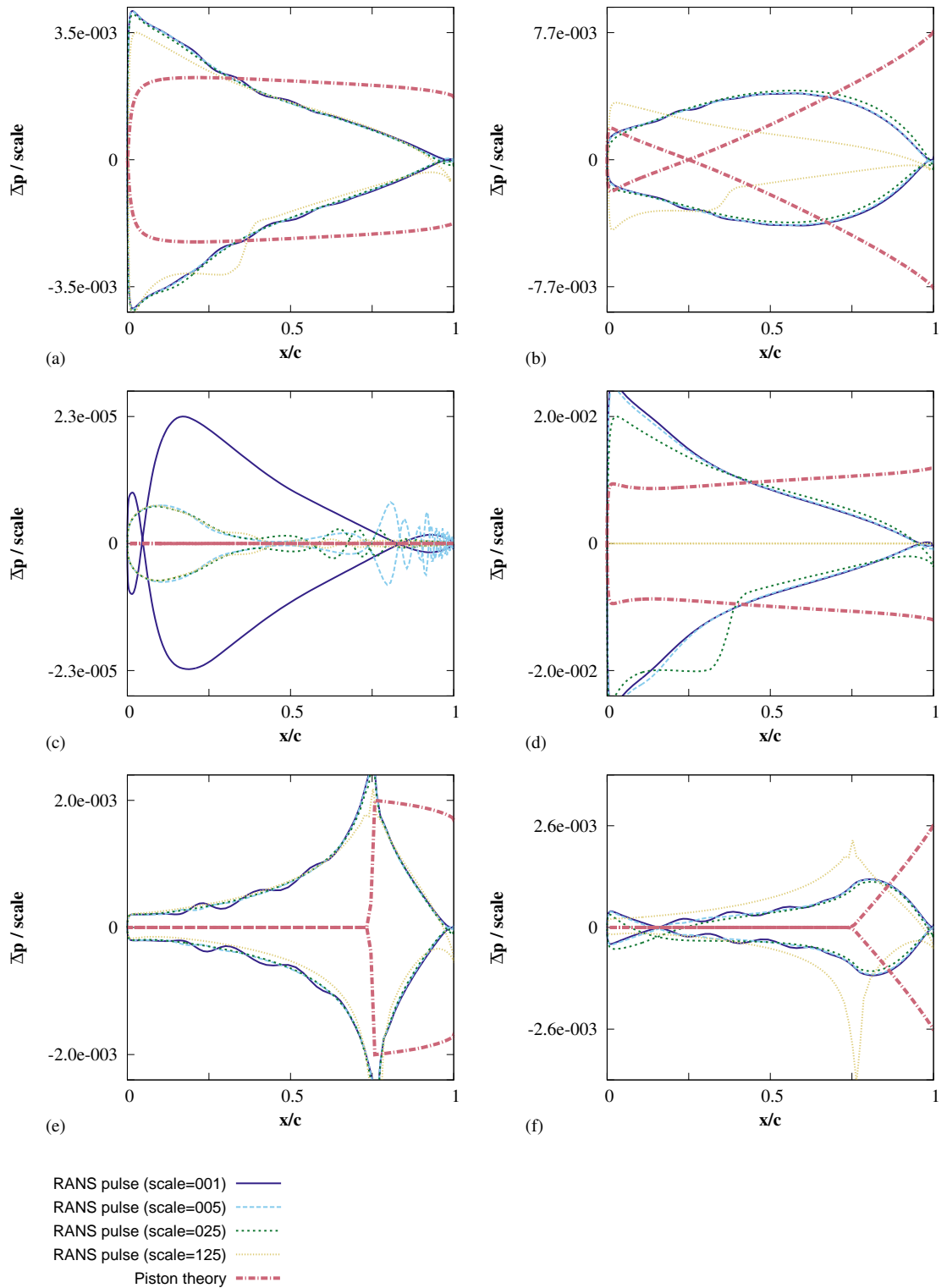


Figure 15. Test case 3 - Scaled pressure response $\bar{\Delta}P$, from Eqn 20 using the viscous wall condition. Responses are shown for (a) α ; (b) $\dot{\alpha}$; (c) h ; (d) \dot{h} ; (e) δ ; (f) $\dot{\delta}$, the pulse magnitudes are given in Table 1.

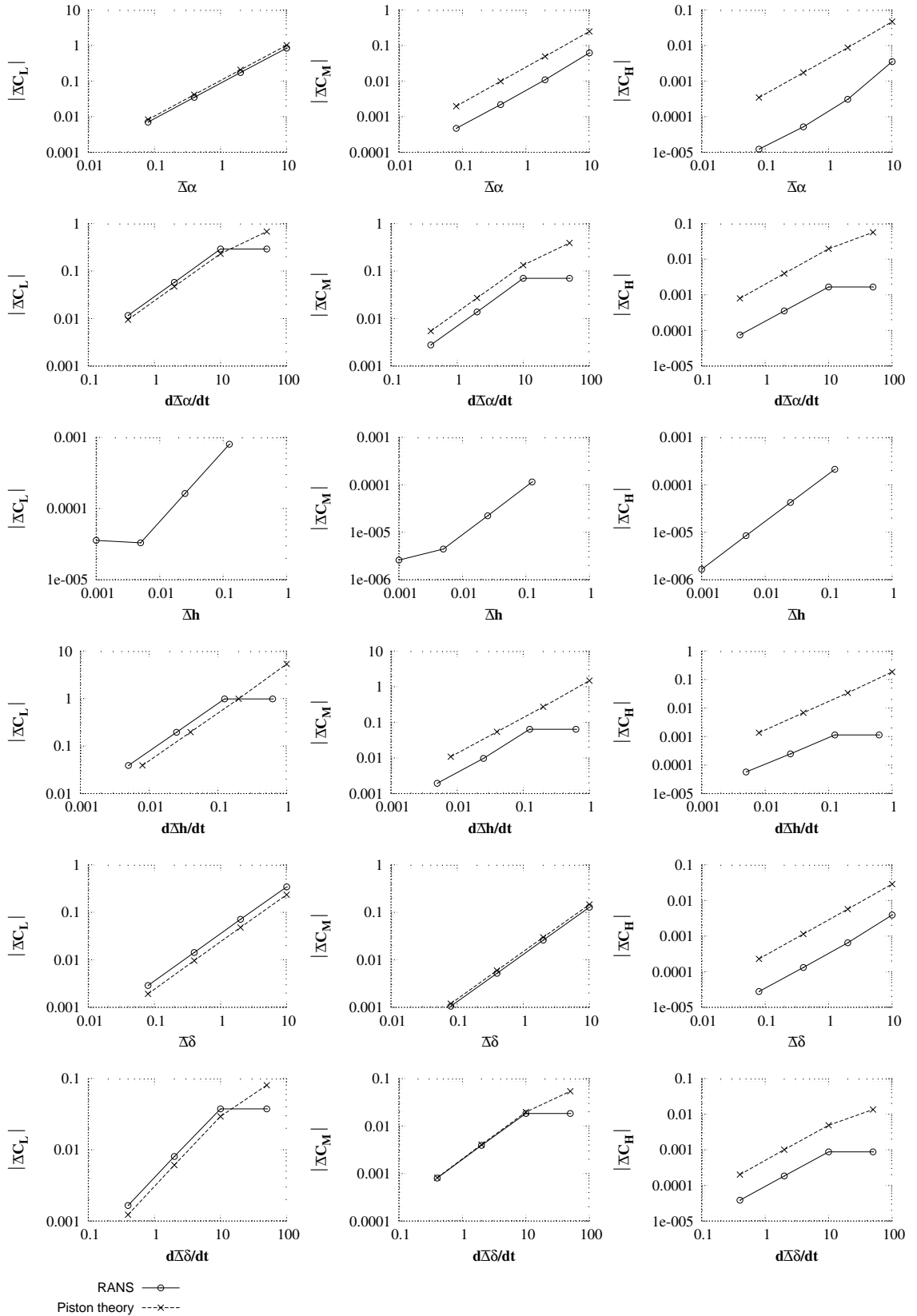


Figure 16. Test case 3 - Integral response (C_l, C_m, C_h). Each row corresponds to the pulse of a row in Table 1 and the points on each plot correspond to the four scales in Table 1